JGR Solid Earth

RESEARCH ARTICLE
10.1029/2020JB020108

Key Points:

- We present an innovative version of the Robust Satellite Techniques able to reduce the proliferation of false-positive thermal anomalies
- A noncasual relation between satellite thermal anomalies and $M_{JMA} \geq 6$ earthquakes affecting Japan in the time span 2005–2015 was found
- Multiparametric approach could accelerate the set-up of a system for time-dependent assessment of seismic hazard

Supporting Information:

- Supporting Information S1

Correspondence to:
N. Genzano,
nicola.genzano@unibas.it

Citation:
Genzano, N., Filizzola, C., Hattori, K., Pergola, N., & Tramutoli, V. (2021). Statistical correlation analysis between thermal infrared anomalies observed from MTSATs and large earthquakes occurred in Japan (2005–2015). *Journal of Geophysical Research: Solid Earth*, *126*, e2020JB020108. https://doi.org/10.1029/2020JB020108

Received 29 APR 2020
Accepted 28 DEC 2020

Statistical Correlation Analysis Between Thermal Infrared Anomalies Observed From MTSATs and Large Earthquakes Occurred in Japan (2005–2015)

N. Genzano[1,2], C. Filizzola[3], K. Hattori[2,4], N. Pergola[3], and V. Tramutoli[1]

[1]School of Engineering, University of Basilicata, Potenza, Italy, [2]Graduate School of Science, Chiba University, Chiba, Japan, [3]Institute of Methodologies for Environmental Analysis, National Research Council, Tito Scalo, Potenza, Italy, [4]Center for Environmental Remote Sensing, Chiba University, Chiba, Japan

Abstract The literature often reports space–time relations between the abnormal variations of different kinds of nonseismological (i.e., geophysical, geochemical, and atmospheric) parameters and the occurrence of earthquakes. The integration of such observations with seismological ones could improve the quality of the seismic hazard assessment in the medium-short term (months to days). Each considered parameter has, in principle, its capabilities to provide useful (and utilizable) information about seismic processes. Therefore, to define a system based on different observations, the first step is to estimate the informative contribution that each considered parameter could provide. In this paper, we will evaluate the potential of Significant Sequence of Thermal Anomalies (SSTAs). In particular, we adopted the broadly used Robust Satellite Techniques (RST) data analysis methodology to identify SSTAs over 11 years (June 2005 to December 2015) of nighttime satellite images acquired by MTSAT satellites over Japan. Aiming at reducing the false-positive rate, we introduced and tested an innovative configuration of the RST, which is here presented. We executed a correlation analysis between SSTAs and Japanese earthquakes with $M_{JMA} \geq 6$ by applying suitable constraints concerning space, time, and magnitude. The analysis highlights (a) the occurrence of just 29 SSTAs in the 11-year period of observation, (b) 18 SSTAs (i.e., 62%) occur in an apparent space–time relation to earthquakes, and (c) 13 of them occur before the quake. Results of the random test analysis, based on error diagrams, confirm a noncasual correlation between "RST-based satellite thermal anomalies" and earthquake occurrences. In particular, for $M_{JMA} \geq 6.5$ earthquakes, probability gain is up to better than 4.3 as compared with the random guess.

1. Introduction

Most of the studies devoted to improving our knowledge on the preparative phases of earthquakes have been based, until now, on the study of single (seismological, geochemical, biological, etc.) observables. A large scientific literature documents the occurrence of anomalous space–time transients of such parameters, which are apparently linked to earthquake preparation phases (see for instance Cicerone et al., 2011; Jiao et al., 2018; Tronin, 2006). However, no demonstration is given concerning the possibility of transforming such observations in methodologies that are actually effective (in terms of precision and reliability of the prediction) in the context of an Operational Earthquake Forecast (OEF) system (see also Geller, 1997, and references therein).

A multiparametric probabilistic approach, devoted to improving the quality of short-term forecast of seismic hazard (rather than providing exact prediction of future earthquakes), today seems the most promising perspective (e.g., Genzano et al., 2020; Tramutoli & Vallianatos, 2020).

To this aim, preliminary studies devoted to qualifying the "predictive" potential of each candidate parameter are of fundamental importance. Starting from long-term correlation analyses, they could provide for each considered parameter the occurrence probability $P(\Delta t, A, M)$ of an earthquake of magnitude $> M$ within a well-defined region A and period of time Δt. On this basis, the weight to attribute to each parameter within a multiparametric system, devoted to dynamically estimating seismic hazard, could be determined.

Such a kind of study should investigate the whole data set of the observations, equally addressing achieved successful rates (i.e., how many anomalies are followed by earthquakes), as well as false-positive rates (i.e., how many anomalies are not followed by earthquakes).

Table 1
Long-Term Statistical Analysis Carried Out Within Different Studies

Parameter	TEMPORAL coverage	STUDIED region	Earthquake magnitude	Reference
Plasma frequency at the ionospheric F2 peak foF2	1994–1999	Taiwan	$M \geq 5$	Liu et al. (2006)
Ionospheric ion density recorded by DEMETER[a]	2004–2010	World	$M \geq 4.8$	M. Li and Parrot (2013)
Ionospheric electron density derived from GIM-TEC map	2000–2010	World	$M \geq 6$	Le et al. (2011)
	1998–2010	Japan	$M \geq 6$	Kon et al. (2011)
	2003–2012	World	$M \geq 7$	Zhu et al. (2014)
	1998–2014		$M \geq 5$	Shah and Jin (2015)
	2000–2013	China	$M \geq 5$	Ke et al. (2016)
	2000–2014	World	$M \geq 6$	Thomas et al. (2017)
	2003–2014		$M \geq 6$	Zhu et al. (2018)
TEC derived from ground-based GPS receivers	2001–2007	Taiwan	$M \geq 5$	Liu et al. (2010)
Subionospheric VLF/LF perturbations	2001–2007	Japan	$M \geq 6$	Hayakawa et al. (2010)
Atmospheric lights and luminous phenomena	1993–2004	Taiwan	$M \geq 5$	Liu et al. (2015)
Earth's outgoing longwave radiation	2009–2019	Taiwan	$M \geq 6$	Fu et al. (2020)
Earth's thermally emitted radiation	2004–2013	Greece	$M \geq 4$	Elefteriou et al. (2016)
	2002–2018	Sichuan (China)		Zhang and Meng (2019)
	2004–2014	Italy		Genzano et al. (2020)
ULF geomagnetic fields	2001–2010	Central Japan	$M \geq 4$	Han et al. (2014, 2017, 2020); Hattori et al. (2013)
ECMWF climatological reanalysis data	1994–2016	Central Italy	$M \geq 5$	Piscini et al. (2017)
GPS measurements of ground deformation	2004–2008	North Island, New Zealand	$M \geq 5.1$	T. Wang et al. (2013)
	1999–2009	Southern California	$M \geq 4.7$	
	1997–2010	Central Japan	$M \geq 5.5$	

[a]A complete list of acronyms is available in Table S5.

Table 1 reports a list of parameters already analyzed on long-term (>5 years) periods in different areas around the world: results of these studies are fundamental to qualify suitable parameters within a system (based on different kinds of parameters) for seismic hazard assessment.

Since the eighties, anomalous fluctuations of Earth's thermal emissions, recorded by Thermal InfraRed (TIR) satellite sensors operating in the spectral region 10–14 μm, have been put in relation with earthquake preparation processes (see Tramutoli, Corrado, Filizzola, Genzano, Lisi, & Pergola, 2015, and references therein).

Among others, the approach, proposed by Tramutoli (1998, 2007) and named Robust Satellite Techniques (RST), has shown the best performance in discriminating anomalous TIR changes presumably related to seismic activity from TIR signal variability caused by other effects (see Tramutoli et al., 2005). The RST methodology has been applied in different world seismic active areas, analyzing time-series of satellite imagery collected by TIR sensors on board polar and geostationary platforms (see Tramutoli, Corrado, Filizzola, Genzano, Lisi, & Pergola, 2015; Tramutoli et al., 2018, for a detailed review).

Moreover, RST has been also broadly used for the same purposes (i.e., to identify possible seismic TIR anomalies) by independent research groups (e.g., Akhoondzadeh, 2013; Bellaoui et al., 2017; Khalili et al., 2019; J. Li et al., 2007; Mukhopadhyay et al., 2021; Xiong et al., 2013), as well as by national space agencies such as DLR (see Halle et al., 2008) and NASA (see Eneva et al., 2008). In particular, the last one recognizes RST as "a better method for detecting preearthquake thermal anomaly."

To explain TIR anomaly appearance, Tronin (1996), Qiang et al. (1997), and Tramutoli et al. (2013) suggested a local greenhouse gas effect as a possible model. It is well known that gases, such as CO_2 and CH_4, are quite transparent to solar radiation and active in absorbing Earth's emitted infrared radiation. At a local scale, they can act as greenhouse gasses because they allow the solar radiation to reach and warm up the Earth's surface. At the same time, they contrast Earth's surface cooling by absorbing and reemitting back (toward the surface) the Earth emitted infrared radiation. As a result, Earth's surface and near-surface atmospheric layers can experiment a warming up, which can be observed even far from the gas sources, depending on the original concentration of emitted gases and local wind regimes. Tramutoli et al. (2009, 2013) simulated the near-surface TIR radiances (measured in terms of brightness temperature), expected as a consequence of increases of CO_2 mixing ratio, from 2 to 20 times its normal value. Quite significant increases of TIR emitted radiation (brightness temperature higher than 10 K) were obtained in correspondence of CO_2 mixing ratio increases of just 2–3 times. In comparison, increases of CO_2 emissions, having orders of magnitude greater, have been observed in relation to major earthquakes' occurrence (e.g., Barka, 1999; Bonfanti et al., 2012; Chiodini et al., 2011). Moreover, it is well known that abnormal quantities of optically active gases like CO_2 and CH_4 can be found alongside seismogenic faults (e.g., Irwin & Barnes, 1980; Tamburello et al., 2018). In fact, the extensive process of microcrack formation supports the increase of such a degassing activity as a consequence of the continuously increasing stress field. This process can be accelerated by the deepwater rise and convective heat flow toward the surface, consequent to crack closure/opening, accompanying the whole (pre and post) seismogenic process (e.g., Scholz et al., 1973). In the same way, TIR anomalies are expected to appear both before and after an earthquake. Izmit seismic event (August 17, 1999; $M_S = 7.8$) represents a clear example of this circumstance. In fact, Barka (1999) and Tramutoli et al. (2005) find out, respectively, an intense degassing activity and satellite TIR anomalies from a few days prior to the main shock up to a number of days after its occurrence. For the M_W 6.3 L'Aquila earthquake on April 6, 2009, similar variations of both TIR and CO_2 gas emissions are reported in the central Italian Apennines directly by ground and, indirectly, by satellite data analyses (Bonfanti et al., 2012; Genzano et al., 2009; Heinicke et al., 2011; Lisi et al., 2010; Martinelli et al., 2020; Pergola et al., 2010). These observations are also supported by the model of fluid migration proposed by Lucente et al. (2010), based on seismic wave velocity analyses. It is worth noting that the role of deformation processes in modulating greenhouse gas emissions depends on local tectonic (see, for instance, Doglioni et al., 2014, and references therein) and geochemical settings, which do not allow us to make generalizations.

Anyway, the above-mentioned model does not exclude that other proposed processes could contribute to the observed thermal anomalies. Among the others, we should mention the models of Freund (2007), who explains TIR anomalies as a consequence of the activation of positive-hole pairs in rocks under stress, as well as the one of Pulinets and Ouzounov (2011), who consider the occurrence of TIR anomalies as one of the expected consequences of the ionization of near-surface air due to intensive radon emission.

In this paper, we examined seismic RST-based TIR anomalies in the context of the Japanese territory. TIR satellite records, acquired over Japan from July 2005 up to December 2015 (11 years) by the satellite sensors JAMI and IMAGER on board the MTSAT-1R and -2 geostationary platforms, respectively, have been analyzed. Aiming at minimizing the occurrence of false positives, we present here, for the first time, an RST-optimized arrangement and its validation. We will discuss results of the correlation analysis of satellite TIR anomalies versus space–time distance and magnitude of earthquakes ($M_{JMA} \geq 6$) that occurred in Japanese territory, looking at the set-up of a multiparametric system for a time-Dependent Assessment of Seismic Hazard (t-DASH; Genzano et al., 2020; Tramutoli et al., 2014).

2. Data and Methods

Thermal anomalies have been identified by analyzing all nighttime (00:30 LT; i.e., 15:30 UTC –1 day) TIR images, acquired at 10.8 μm (10.3–11.3 μm) by JAMI sensor on board MTSAT-1R satellite in the period June 2005–2010 and by IMAGER sensor on board MTSAT-2 satellite in the period July 2010 to December 2015. Those images belong to the gridded data set at a spatial resolution of 0.04° provided by CEReS of Chiba University.

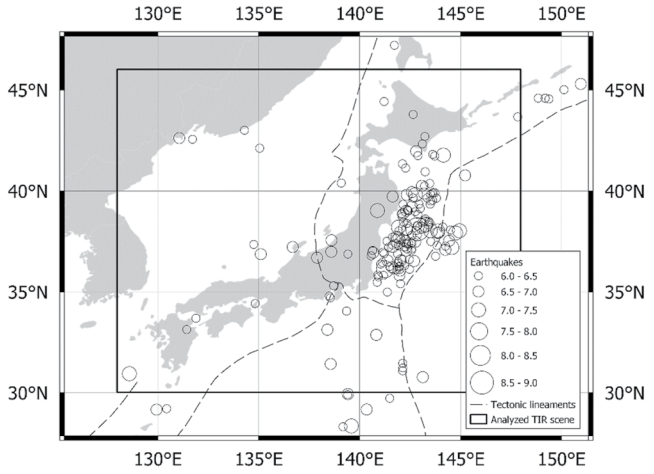

Figure 1. Investigated area. The rectangular black solid line contains the area of the analyzed MTSAT TIR scene; circles indicate earthquakes with $M_{JMA} \geq 6$ occurred from June 15, 2005, to January 31, 2016, inside the wider area 27°N–49°N and 125°E–151°E.

Figure 1 shows the investigated area (latitude 30–46°N and longitude 128–148°E), which covers the Japanese territory. Here, the earthquakes that occurred in an area which is 3° greater than the investigated region in the period June 15, 2005 to January 31, 2016 are also shown. As reported in the seismic catalog of the JMA (Japan Meteorological Agency, 2021), there are 229 events with $M_{JMA} \geq 6$ and 79 events with $M_{JMA} \geq 6.5$, occurred in the considered time period and selected geographic area.

The RST approach proposed by Tramutoli (1998, 2007) allowed us to identify TIR anomalies possibly related to the occurrence of earthquakes. The essence of such a change detection method is that a variation of the signal is considered as "anomalous" when it differs significantly from its "normal" behavior. This behavior is estimated by exploiting all information coming from time-series of satellite homogenous (i.e., same sensor, similar time of the day, and the same month of the year) imagery. An accurate description of the RST approach can be found in Eleftheriou et al. (2016).

In this study, to identify TIR anomalies, we used the statistically based Robust Estimator of TIR Anomalies (RETIRA; Filizzola et al., 2004; Tramutoli et al., 2005) index, called in Genzano et al. (2020) $RETIRA_{box}$, which is computed by the following expression (Equation 1):

$$\otimes_{\Delta T_{box}}(x,y,t) \equiv \frac{\Delta T_{box}(x,y,t) - \mu_{\Delta T_{box}}(x,y)}{\sigma_{\Delta T_{box}}(x,y)} \quad (1)$$

where

- (x, y) are the geographical coordinates corresponding to the center of the pixel.
- t is the satellite acquisition time with $t \in \tau$, being τ the temporal domain including all the nighttime MT-SAT images collected at 00:30 LT from June 2005 to December 2015.
- $\Delta T_{box}(x,y,t)$ is the spatial average of $\Delta T(x,y,t)$ within a region of 3 × 3 pixels centered at location (x,y). Its computation takes place only if at least 55% of pixels within the box are clear and not close to clouds (cloud-free boxes). The One-channel Cloudy-radiance-detection Approach (OCA; Cuomo et al., 2004) algorithm identified cloudy pixels.
- $\Delta T(x,y,t) = T(x,y,t) - T(t)$ is the difference between the punctual values of the TIR brightness temperature $T(x,y,t)$ and the daily spatial average $T(t)$. It should be stressed that $T(t)$ computation takes account only of cloud-free values of the whole investigated region, which is part of the identical category (i.e., only sea or land pixels if (x,y) is on the sea or land, respectively).
- $\mu_{\Delta T_{box}}(x,y)$ and $\sigma_{\Delta T_{box}}(x,y)$ are the values of time average and standard deviation of $\Delta T_{box}(x,y,t)$ reckoned on cloud-free boxes belonging to the chosen data set ($t \in \tau$).

The choice to use $\Delta T_{box}(x,y,t)$ should reduce the spurious TIR anomaly appearances due to sporadic and spatially localized events (e.g., due to fires or industrial accidents) and preserving and emphasizing concurrently those anomalies that have an appreciable spatial extension, as expected for TIR anomalies possibly associable with earthquake preparation phases.

We adopted here the improved RST preprocessing phases proposed by Eleftheriou et al. (2016) to bring down the possible negative impact of the meteorological clouds on the computation of reference fields and the consequent proliferation of possible false positives. In fact, such effects could be particularly significant in a geographical context such as Japan, subject to a variety of climatic conditions within a relatively small land area. In addition, it is also affected by several phenomena such as the monsoons in the southern part during summer and early autumn, typhoons in the Pacific side from August to October, and the influence of atmospheric pressure of the Sea of Okhotsk in the northern part of the Sea of Japan.

So, for each month of the year, we computed two images ($\mu_{\Delta T_{box}}$ and $\sigma_{\Delta T_{box}}$ images) used as "reference images" (i.e., RST reference fields) for the calculation of the $RETIRA_{box}$ index. They are representative of the expected thermal conditions.

Using such reference fields, we calculated *Thermal Anomaly Maps* (TAMs) for all MTSAT-1R/2 TIR images (i.e., 3,747 in the period June 2005 to December 2015); TAMs report the value of $\otimes_{\Delta T_{box}}(x,y,t)$ for all cloud-free locations. From now on, we consider as *Thermal Anomalies* (TAs) those locations with $\otimes_{\Delta T_{box}}(x,y,t) \geq 3.5$—that is, with signal excess $\Delta T_{box}(x,y,t) - \mu_{\Delta T_{box}}(x,y) \geq 3.5\,\sigma_{\Delta T_{box}}(x,y)$.

Like in previous studies (see Tramutoli, Corrado, Filizzola, Genzano, Lisi, & Pergola, 2015; Tramutoli et al., 2018, and references therein), we carried out a preliminary space–time persistence analysis on the TAs before qualifying them as Significant Thermal Anomalies (STAs). In fact, deriving from a statistical approach, the $RETIRA_{box}$ index can be exposed to a proliferation of signal outliers (see Tramutoli et al., 2005). Aliano, Corrado, Filizzola, Genzano, et al. (2008), Aliano, Corrado, Filizzola, Pergola, et al. (2008), Filizzola et al. (2004), and Genzano et al. (2009) report examples of TIR anomalies caused by specific natural and observational conditions. In all cases, these TAs show a particular spatial distribution and a short-lived character in the time domain. These features allow us to identify and discriminate them from TAs spatially and temporally persistent, which may be associated with an impending seismic event. So, only STAs that are persistent in a restricted space–time domain can belong to a Significant Sequence of Thermal Anomalies (SSTAs).

As discussed in Eleftheriou et al. (2016), Genzano et al. (2015, 2020), and Tramutoli, Corrado, Filizzola, Genzano, Lisi, Paciello, et al. (2015), an SSTA occurs when the following requirements are satisfied:

- *Relative intensity*. TAs should have a value of $\otimes_{\Delta T_{box}}(x,y,t) \geq K$ (in this paper, $K = 3.5$).
- *Discard of spurious effects*. Portions of the scene (i.e., land or sea) of the TAMs with a large cloud cover, navigation errors (Filizzola et al., 2004), and known spurious effects (see Aliano, Corrado, Filizzola, Genzano, et al., 2008; Eleftheriou et al., 2016; Genzano et al., 2009, 2015 for more details) are discarded from the subsequent analyses; about cloud cover, in this study, we consider useful only portions of the scene having a fraction of cloudy pixels less than 80% of those belonging to the same land/sea class.
- *Minimum spatial extension*. Each STA has to cover at least an area of 150 km^2 within a region of 1° × 1° around (*x*,*y*).
- *Persistence in space–time domain*. STAs are 1° distant maximum from each other (spatial persistence) and reappear at least another time in the 7 days preceding/following *t* (temporal persistence).

Figure 2(a) shows an example of SSTA, which appeared in the Pacific Sea on October 18–19, 2013. Although both TIR images show cloudiness in the southern part, the highlighted TIR anomalies are not due to the cold spatial average effect (Aliano, Corrado, Filizzola, Genzano, et al., 2008; Genzano et al., 2009), as confirmed by the cloud coverage analysis reported in Figure 2(b).

3. Data Analysis

3.1. Seismic Catalog Filtering

We performed the correlation analysis presented in the following sections considering the seismic events with $M_{JMA} \geq 6$ that occurred in the studied area/period. As Michael (1997) highlights, earthquake clustering could have an effect on results. Unlike those studies (e.g., seismological) aiming at assessing seismic hazard, where the declustering of an earthquake catalog is a fundamental preliminary analysis, and its quality could influence the results of subsequent analyses, studies based on nonseismological parameters are less influenced by the method that is used for earthquake declustering.

In this study, we adopted specific criteria for selecting earthquakes to be considered in the correlation analysis. Since more than one earthquake can occur in a time span *ts* in neighboring areas, for each seismic event that occurred in *ts*:

(a) we computed the corresponding Dobrovolsky radius (Dobrovolsky et al., 1979), , where M*i* is the magnitude of the *i*th earthquake;

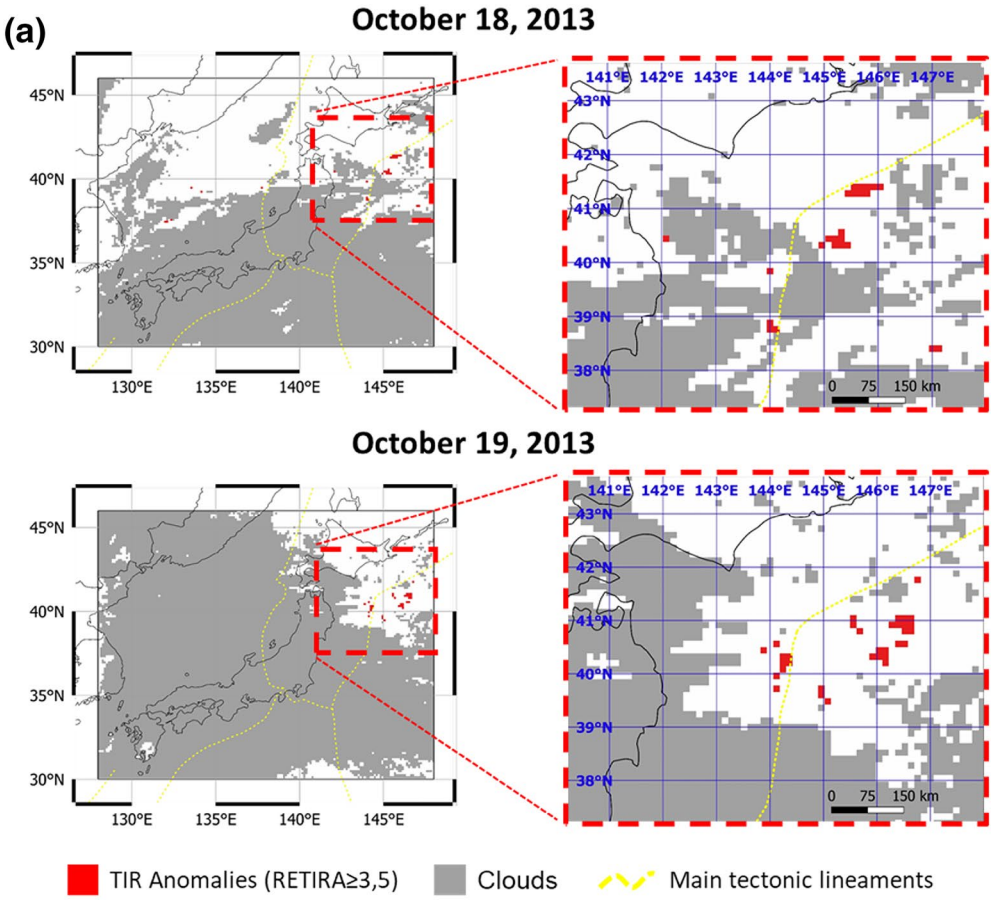

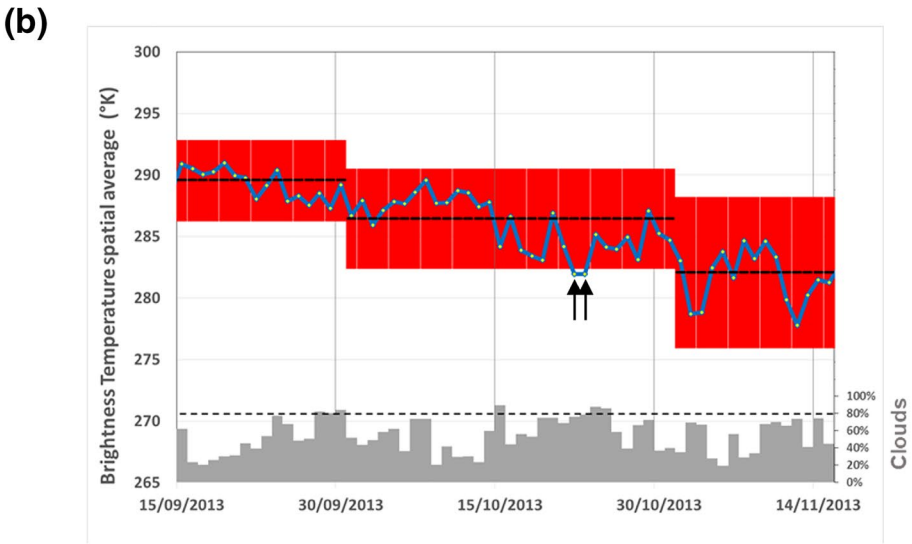

Figure 2. (a) TAMs where STAs appear with an appreciable extension (i.e., at least 150 km^2) and a space–time persistence on October 18 and 19, 2013, over the Pacific Sea. (b) The analysis was necessary to identify TAs due to meteorological effects. The yellow circles indicate the daily spatial averages $T(t)$ over sea computed on cloud-free pixels; the black lines indicate the temporal averages (μ_T); the red zone defines the $\pm 2\ \sigma_T$ bounds used for excluding images affected by the *cold spatial average effect* (like the ones indicated by the black arrows), which have been computed by using all images available in the period 2005–2015 during the same month; the gray bars represent the cloud percentage over the sea part of the scene. TAMs, Thermal Anomaly Maps; STAs, Significant Thermal Anomalies; TAs, Thermal Anomalies.

(b) we sorted events by decreasing magnitude and increasing time of occurrence;
(c) starting from the first event in the list, we excluded all the events falling within its Dobrovolsky radius;
(d) we repeated the process for all the survived events in the list until all the events have been evaluated.

Figure S1 in supporting information shows some examples.

For this study, we generated two different filtered catalogs:

- Daily filtered catalog, where $ts = 1$ day. We used this catalog for a preliminary evaluation of comparative performance between the traditional RST analysis and its optimized arrangement, here presented. This filtered catalog consists of 157 events with $M_{JMA} \geq 6$ and 58 events with $M_{JMA} \geq 6.5$.
- Monthly filtered catalog, where $ts = \pm 30$ days. We used this catalog to evaluate if the high seismicity of the Japanese region could affect results concerning the RST-optimized arrangement. This filtered catalog consists of 82 events with $M_{JMA} \geq 6$ and 35 events with $M_{JMA} \geq 6.5$.

3.2. Correlation Analysis Between TIR RST-Based Anomalies and Earthquake ($M_{JMA} \geq 6$) Occurrences

We applied the aforementioned rules to all MTSAT TIR images, which are available in the period June 2005 to December 2015, and we identified 60 SSTAs (spread over 132 different TIR images, i.e., 3.5% of the total available TIR images).

We evaluated the possible correlations between the SSTA appearances and location, time, and magnitude of the earthquakes belonging to the daily filtered catalog. To this aim, we applied empirical rules which were established taking account of both previous studies (see Tramutoli, Corrado, Filizzola, Genzano, Lisi, & Pergola, 2015; Tramutoli et al., 2018, and references therein) and physical models (e.g., Tramutoli et al., 2013) to date proposed to explain the TA appearances before and after large earthquakes. Furthermore, the defined validation rules, which should drive the retrospective correlation analysis, match those rules used by the CSEP project (Schorlemmer et al., 2018).

Following such rules, we consider each STA observed in a geographical site (x,y), at the time t, and belonging to a previously identified SSTA, in correlation with a seismic event of $M \geq 6$, if it occurs within a defined:

- *temporal window*, that is, up to 30 days after (preearthquake anomaly) the last appearance of TAs, or until 15 days before (postseismic/coseismic anomaly) the first one and
- *spatial window*, that is, within a distance RD from the TAs forming the SSTA, where $R_D = 10^{0.43M}$, that is the Dobrovolsky radius (Dobrovolsky et al., 1979).

Figure 3 illustrates a schematic view of the applied rules. For the SSTA of October 18–19, 2013, a space–time volume, within which to verify the possible relations between TAs and seismic events, has been defined for different classes of possible earthquake magnitudes (here only $M \geq 6$ and 6.5 are drawn by a different color). The earthquakes that satisfy the above definition are the red dots. In that case, the STAs appearing off the north-eastern coast of Japan on October 18 and 19, 2013, were followed by one earthquake of magnitude 7.1. It occurred 8 days (i.e., October 26, 2013) after the first TA appearance in the Pacific Ocean.

On this basis, applying the aforesaid correlation rules to the identified SSTAs (i.e., 60) on the used MTSAT TIR data set, the analysis highlights that 50% of SSTAs are apparently related in space and time to earthquakes ($M_{JMA} \geq 6$), and 50% not (false positives). We should underline that it is not possible to establish an association one-to-one between one SSTA and one specific earthquake that occurred on the same day; in most cases, the predictive power of the considered parameter can be judged only in a collective sense (Nakatami, 2020).

3.3. Reduction of the False-Positive TIR Anomalies

In this paper, the newly applied RST analysis uses a different criterion to build the historical data set of TIR satellite images in order to lower the number of false-positive occurrences. Up to now, in the previous RST applications, we computed the RST reference images (i.e., time average and standard deviation) using

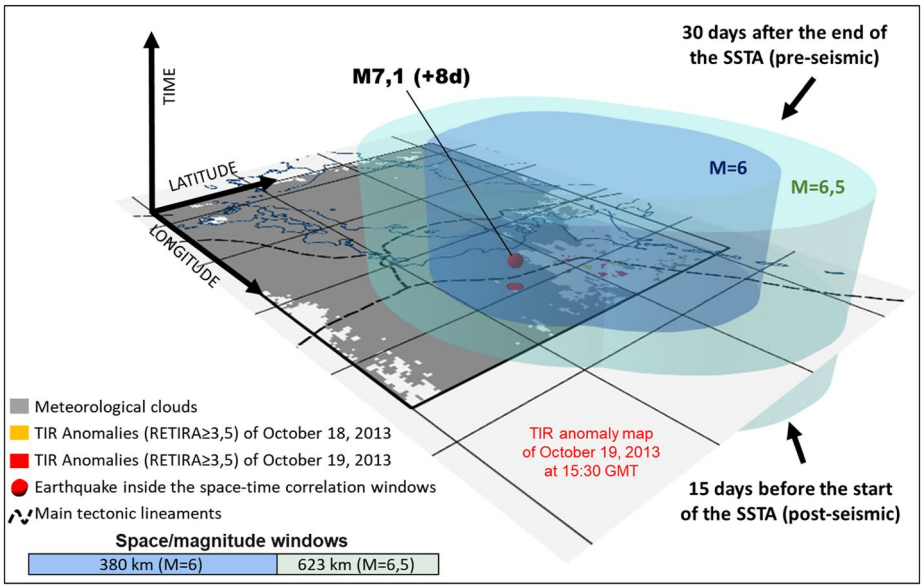

Figure 3. A schematic view of the applied correlation rules. The colored cylinders around the identified SSTA (October 18 and 19, 2013) represent the alerted space–time volumes for different classes of earthquake magnitude (see text for more details). In addition to STAs of October 19 (represented by red pixels), STAs of October 18 (represented by orange pixels) are superimposed to the TIR anomaly map of October 19, 2013, as well. The red ball (with its projection on the map) represents the earthquake inside the correlation rules, and the label indicates its magnitude and temporal distance (in days) from the first STA appearance (i.e., October 18, 2013). SSTA, Significant Sequence of Thermal Anomaly; STAs, Significant Thermal Anomalies; TIR, Thermal InfraRed.

the historical data sets of TIR images built by records collected in the same calendar month (*fixed-monthly window criterion*, FWC). Therefore, for each month, we generated two images (μ and σ) taken into account to identify the TIR anomalies. For most of the days of a month (i.e., those of the middle part of the month), these two images are very representative of the expected (i.e., normal) conditions, especially for long, homogenous, and densely populated time-series of TIR satellite records. However, in specific circumstances (e.g., abrupt changes of the meteorological factors or poor availability of cloud-free scenes during a month), a monthly reference image could not be suitable to represent conditions that can significantly change, from the first and the last day of a month. Consequently, TIR anomalies could proliferate with effects that could be particularly significant in the days in the beginning and/or at the end of a month (when the rest of the month is usually colder/warmer depending on the season), and when the reference fields are computed using not adequately rich historical data sets.

In this paper, we present a different criterion to compute the RST reference fields. Rather than using an FWC, we used a temporal window of 30 days (i.e., ±15 days) around each analyzed day of the year (*moving window criterion*, MWC) to build (366 × 2 instead of 12 × 2) reference fields. In this way, we computed 732 reference field images (two, μ and σ, images for each day of the year), rather than the 24 monthly reference field images (two, μ and σ, images for each month of the year). This allows us to compare the TIR records with the most appropriate reference field. In some geographical areas and periods of the year, this choice could significantly reduce the proliferation of thermal anomalies occurring in the beginning/at the end of a month. Retracing the same above-described steps, we performed a new correlation analysis between SSTAs and the earthquakes belonging to the daily filtered catalog. The use of the same catalog previously employed in assessing RST_{FWC} performance permitted us to better judge the achieved improvements of RST_{MWC} as compared with RST_{FWC}.

This new analysis highlighted that 62.1% of the 29 identified SSTAs (in this case, spread over 69 different TIR images, i.e., 1.8% of the total available TIR images), in the period June 2005 to December 2015 over the Japanese region, are apparently associated in space and time with reported seismic events ($M_{JMA} \geq 6$, Table 2).

Table 2
Summary of the Correlation Analysis

Id	SSTA place	SSTA period	SSTA type	In correlation with EQs	EQ magnitude JMA and time lag (days) from the first ÷ last TIR anomaly appearances
1	Hokkaido	Dec 20, 2005 to Jan 13, 2006	POST EQ	Y	6.1 (–3 ÷ –27)
2	Chugoku	Dec 23–24, 2005		N	
3	Chubu	Jan 25–31, 2006		N	
4	North Japan Sea	Jan 19–20, 2006		N	
5	South Russia	Feb 4–8, 2007	PRE EQ	Y	6.2 (+33 ÷ +29)
6	Shikoku	Mar 29–31, 2007	POST EQ	Y	6.9 (–4 ÷ –6)
7	Chubu	May 27–29, 2008	PRE EQ	Y	7.2 (+18 ÷ +16)
8	South Russia	Nov 6–7, 2008		N	
9	Hokkaido	Jan 14–29, 2009		N	
10	South Russia	Jan 27–29, 2009		N	
11	offshore East Hokkaido	Feb 14–15, 2009		N	
12	Chubu	Nov 9–15, 2009		N	
13	South Korea	Nov 13–14, 2009	POST EQ	Y	6.8 (–14 ÷ –15)
14	Kyushu	Feb 8–10, 2010		N	
15	Offshore East Hokkaido	Feb 4–10, 2011	PRE EQ	Y	7.3 (+33 ÷ +27), 6.8 (+34 ÷ +28), 9 (+35 ÷ +29), 6.8 (+36 ÷ +30)
16	South Korea	Nov 28 to Dec 1, 2011		N	
17	Offshore East Hokkaido	Apr 26–30, 2012	PRE EQ	Y	6.5 (+24 ÷ +20), 6.1 (+28 ÷ +24)
18	Japan Sea (offshore Tohoku)	Jul 20–21, 2012		N	
19	Hokkaido	Sep 14–18, 2012	PRE EQ	Y	6.3 (+18 ÷ +14)
20	Kansai	Mar 18–19, 2013	PRE EQ	Y	6.3 (+26 ÷ +25), 6.2 (+30 ÷ +29)
21	Pacific Sea	Mar 23–26, 2013	PRE EQ	Y	6.2 (+10 ÷ +7), 7 (+27 ÷ +24)
22	Kanto	Apr 18–22, 2013	PRE & POST EQ	Y	6.3 (–5 ÷ –9), 6.2 (–1 ÷ –5), 6.4 (+3 ÷ –1), 6 (+30 ÷ +26)
23	Japan Sea (offshore Chugoku)	Aug 20–26, 2013	PRE EQ	Y	6.8 (+15 ÷ +9)
24	Pacific Sea	Oct 18–19, 2013	PRE EQ	Y	7.1 (+8 ÷ +7)
25	Tohoku	Jan 16–21, 2015	PRE EQ	Y	6.9 (+32 ÷ +27), 6.5 (+35 ÷ –)
26	South Russia	Jan 25–29, 2015	PRE EQ	Y	6.9 (+23 ÷ +19)
27	Offshore East Hokkaido	Mar 4–8, 2015	POST EQ	Y	6.9 (–15 ÷ –19), 6.5 (–12 ÷ –16)
28	Shikoku	Nov 6–9, 2015	PRE EQ	Y	7.1 (+8 ÷ +5)
29	Chugoku	Nov 21–23, 2015	POST EQ	Y	7.1 (–7 ÷ –9)
			29 SSTA	**18 Y 11 N**	**62.1% Y 37.9% N** (for $M \geq 6$)
				13 Y 16 N	44.8% Y 55.2% N (for $M \geq 6.5$)

Comparing the two independent RST analyses, attention should be focused on the diminution of:

- the number of SSTAs from 60 (highlighted by using the traditional RST analysis, RST_{FWC}) to 29 (highlighted by using the proposed innovative RST analysis, RST_{MWC});
- the false-positive SSTAs from 30 (corresponding to 50% of all SSTAs) to only 11 (corresponding to 37.9% of all SSTAs).

Table 3 shows a comparison between the space–time distribution of false positives of both the RST analyses. We should point out that, as expected, most of the SSTAs disappear during the periods and geographic areas that are subject to abrupt climatologically changes, such as in the fall–winter transition period (i.e.,

Table 3
Schematic Representation of the Space–Time Distribution of False Positives

	China, South Russia	Hokkaido, North Japan Sea	Tohoku	Kanto, Chubu	Kansai, Chugoku Shikoku	Kyushu	South Korea	Central Japan Sea	South Pacific Sea	Total for month
Jan	**2** (1)	**1** (0)		**1** (1)	**0** (1)	**0** (1)				**4** (4)
Feb		**1** (0)				**1** (0)				**2** (0)
Mar										**0** (0)
Apr			**0** (1)							**0** (1)
May										**0** (0)
Jun		**0** (1)		**0** (1)						**0** (2)
Jul								**1** (1)	**0** (1)	**1** (2)
Aug					**0** (1)				**0** (1)	**0** (2)
Sep										**0** (0)
Oct		**0** (1)				**0** (1)				**0** (2)
Nov	**1** (5)	**0** (2)		**1** (0)		**0** (1)	**1** (2)	**0** (1)	**0** (1)	**3** (12)
Dec	**0** (1)			**0** (1)	**1** (1)	**0** (1)		**0** (1)		**1** (5)
Total for region	**3** (7)	**2** (4)	**0** (1)	**2** (3)	**1** (3)	**1** (4)	**1** (2)	**1** (3)	**0** (3)	**11** (30)

Numbers in bold indicate false positives recorded by RST_{MWC}, while numbers within parentheses indicate the corresponding false positives in the case of RST_{FWC}.

November) in the NW area of the investigated scene (i.e., South Russia). Moreover, we recorded a strong reduction of false positives (up to zero) in selected areas such as Tohoku and the Pacific Ocean. In addition, among SSTAs associable with an earthquake occurrence, RST_{MWC} confirms a dominance of preseismic ones (13 out of 18) (Figure 4).

We carried out a random test analysis with the purpose of both evaluating the quality of the achieved results and the potential informative contribution of the "RST-based satellite thermal anomalies" parameter to a multiparameter system devoted to the evaluation of the seismic hazard in the short term. Such an analysis should also highlight if SSTAs (both preevents and postevents) appear related to earthquakes just because of the high seismicity of the studied region and/or because of the used correlation space/time rules (eventually set too large).

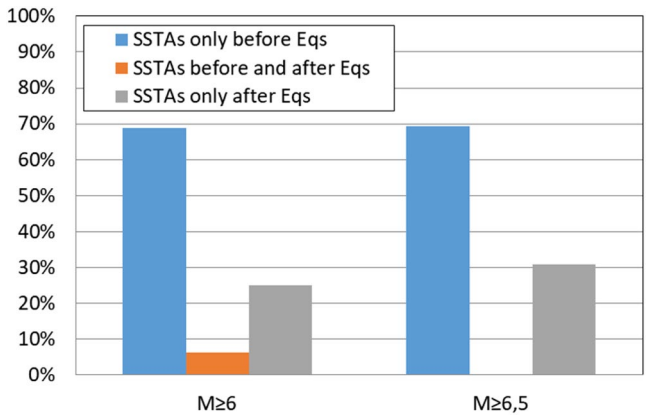

Figure 4. The RST_{MWC}-based SSTA distribution compared to the occurrences of seismic events of magnitude 6 and 6.5. SSTA, Significant Sequence of Thermal Anomaly.

We have taken the Molchan approach (Molchan, 1997, and references therein) into account as a reference method for the verification of the actual value of an SSTA-based, as compared with a random-based, alarm function.

In the past, the Molchan test was widely used as a diagnostic tool to evaluate earthquake-forecasting methods based on the seismicity maps. These maps are obtained using the catalogs of historical earthquakes, seismotectonic regionalization methods, smoothing techniques, and so on (e.g., Molchan, 2012). Such a kind of map represents a "reference model," and it should reflect "the current knowledge about the seismic process" (Shebalin, 2018). It should be noted that, in the Molchan diagram (or error diagram), the reference model is often interpreted as the fraction of the space–time region occupied by alarms (Kossobokov & Shebalin, 2003), and "the selection of the correct model is the most important part of the testing" (Molchan, 2012). In the diagram, τ denotes the reference model, and it is compared with the fraction ν (i.e., missing rates) of the earthquakes that occur outside the alarmed space–time regions.

The method proposed by Molchan (1990, 1991) and Molchan and Kagan (1992) can be considered as a simplistic analysis as compared to the methods that extended it, for example, the Area Skill Score (Zechar & Jordan, 2008, 2010). Moreover, Molchan's diagram should be applied in the absence of observational gaps (in our case, represented by clouds, which we cannot avoid). Despite those considerations, we preferred to adopt, on the basis of the specific features of the investigated parameter (i.e., RST-based SSTAs), the customized Molchan's error diagram proposed by Shebalin et al. (2006), rather than to use an approach based on a likelihood test. In fact, such a kind of test cannot be used in the case of models with a nonprobabilistic alarm function (Shebalin et al., 2014).

It should be noted that the alarm functions, focused on predictive identification of future seismic events with a chosen minimum magnitude threshold, could also be used for more complex forecasts (see Zechar & Jordan, 2008). On the contrary, the purpose of our random test analysis is to understand whether a noncasual relation exists (or not) between the identified satellite thermal anomalies and earthquake occurrence for the Japanese region in the period June 2005 to December 2015. Therefore, a possible high rate of missed earthquakes should not be considered as a problem because the lack of continuity, inherent in the specific observational methodology, does not affect the predictive power of the SSTA parameter. In fact, the goal is to contribute to increasing the reliability of each single forecast by reducing false-positive rates rather than predicting all earthquake occurrences.

In our case, the error diagram plots the percentage of the earthquakes that are not preceded/followed by SSTAs ν_{EQ} (i.e., missed EQ) versus the percentage of the alerted space–time volume τ_{SSTA}. We computed them using the expressions 2 and 3 (see Eleftheriou et al., 2016, for more details):

$$\nu_{EQ}(M) = \frac{\text{number of EQs with magnitude} \geq M \text{ outside the space–time correlation window (missed)}}{\text{total number of EQs with magnitude} \geq M \text{ occurred within the whole space} \times \text{time volume}} \quad (2)$$

$$\tau_{SSTA}(M) = \frac{\text{alerted space} \times \text{time volume for EQs with magnitude} \geq M}{\text{whole investigated space} \times \text{time volume}} \quad (3)$$

Additionally, we calculated the probability gain (Aki, 1989) $G = (1 - \nu_{EQ})/\tau_{SSTA}$ as well as the confidence limit curves, based on the null-hypothesis (see Kossobokov, 2006 for more details), at levels of 95% surrounding the diagonal of the random guess.

Figure 5(a) shows the result of the error diagram. Here, we also evaluated the achieved results of Molchan's analysis in comparison with the results of analyses obtained by using 50 synthetic catalogs, where events have the same locations and magnitudes as in the daily filtered catalog but randomly generated occurrence time (see Figures S2 and S3 in supporting information for more details). Our findings indicate that

- the results are in the optimistic zone with a "significant" deviation from random guessing (i.e., confidence levels of 95%);
- the results about the synthetic catalogs surround the random guess line (for the sake of simplicity, we report just the mean values, full details are in supporting information); not only the mean values but also all results achieved by simulated catalogs reject the null-hypothesis at the significant level $\alpha = 5\%$; and
- probability gain reaches 2 (for $M \geq 6$ preearthquakes' and postearthquakes' SSTAs) up to 4.3 (for $M \geq 6.5$ only preearthquakes' SSTAs) as compared to the random guess.

Figure 5(a) shows that alarms have been proven to be better than the random guess from the view of events, but in order to verify if it is the same from the view of alarms, we built an ad hoc error diagram (Figure 5(b)), considering

$$\nu_{SSTA(M)} = \frac{\text{number of SSTAs not corresponding to EQs with magnitude} \geq M \text{ (false positive)}}{\text{total number of SSTAs identified within the whole space} \times \text{time volume}} \quad (4)$$

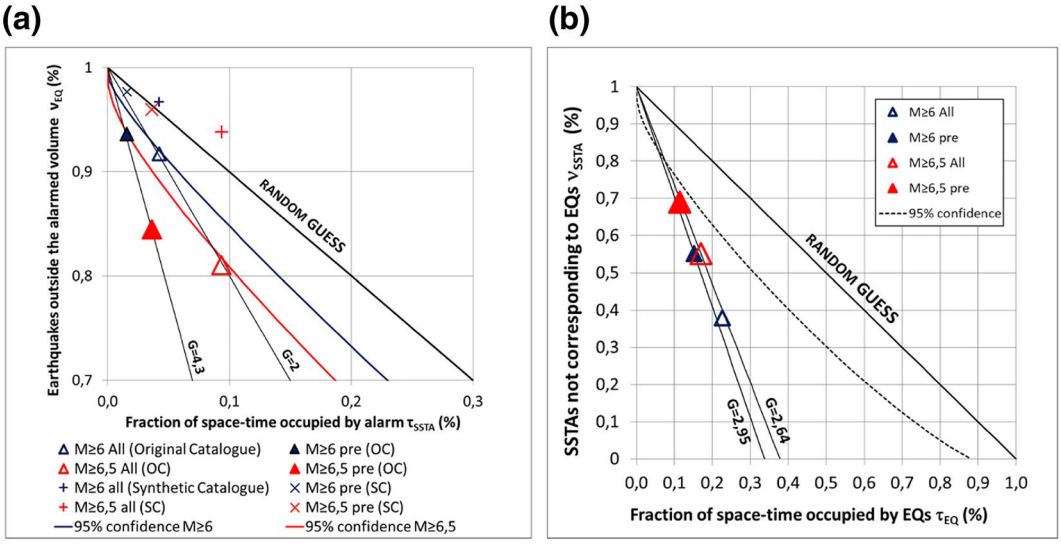

Figure 5. Error diagrams from the point of view of the events (a) and alarms (b) identified by RST_{MWC} on the whole studied period (June 2005 to December 2015). In (a), the graph is zoomed to emphasize the achieved results. Empty triangles refer to the seismic events, within alerted volumes corresponding to $M_{JMA} \geq 6$ and 6.5, which occurred after or before SSTA appearances (preseismic and postseismic anomalies). Full triangles refer just to the events occurred after the SSTA appearances (only preseismic anomalies). Similarly, blue and red cross/plus symbols indicate the mean values of the results concerning the analyses performed by using different synthetic catalogs (see Table S1 in supporting information). Blue and red lines indicate the confidence limit curves surrounding the diagonal of random guess for earthquakes with $M_{JMA} \geq 6$ and 6.5, respectively. In this study, confidence levels of 95% are used to indicate the "significant" deviance from the random guessing function. In (b), full triangles refer to the SSTAs which are not followed by events with $M_{JMA} \geq 6$ and 6.5. Empty triangles refer to SSTAs not followed or preceded by seismic events. The dashed line indicates 95% confidence surrounding the random guess for the 29 identified SSTAs. For both diagrams, minimum and maximum probability gains (G) are reported. SSTA, Significant Sequence of Thermal Anomaly.

$$\tau_{EQ}(M) = \frac{\text{space} \times \text{time volume occupied by EQs with magnitude} \geq M}{\text{whole investigated space} \times \text{time volume}} \quad (5)$$

We computed "space × time volume occupied by EQs with magnitude ≥ M" considering

- temporal window: from 30 days before up 15 days after the earthquake occurrences (for a total of 46 days) and
- spatial window: $R_D = 10^{0.43M}$, that is the Dobrovolsky radius (Dobrovolsky et al., 1979).

Figure 5(b) highlights that SSTAs are better than the random guess even from the alarm point of view. Also for this test, a probability gain was computed as $G = (1 - \nu_{SSTA})/\tau_{EQ}$. Obtained values reach 2.95 (for SSTAs that precede earthquakes with $M \geq 6$) as compared to the random guess.

Achieved results are encouraging, even if they represent just the minimal level of the actual parameter performance. In fact, they should also be evaluated considering two main aspects:

- persistent clouds produce space/time data gaps and, consequently, a lot of possible missed events when data, like in this study, are frequently (65% of the total) masked by clouds and
- the degassing process can strongly vary in terms of quantity, geochemical species, and flux rates, depending on local geotectonic setting as well as geochemical/lithological features; in this way, it can be supposed that not all events are preceded/followed by TIR anomalies as a result of the variable presence/intensity of the degassing activity.

Additionally, in order to verify whether or not the presence of earthquake clusters could have influenced the achieved results, the possible relation between identified SSTAs (i.e., 29 sequences) and seismic events has

been verified taking account of a catalog filtered on a monthly basis instead of a daily basis. This correlation analysis shows that 17 out of 18 SSTAs (previously highlighted in an apparent space–time relation with events with $M_{JMA} \geq 6$) still exhibit a space–time relationship with earthquakes (see the summary reported in Table S2 of supporting information).

Similarly to what was done previously, the error diagram was built taking account of both the monthly filtered catalog and synthetic catalogs generated starting from it. Figure 6(a) reports the achieved results. Concerning the filtered catalog, the results are in the optimistic zone with a "significant" deviation from random guessing, showing a probability gain up to 4.75 (for $M \geq 6.5$ earthquakes), as compared to the random guess. On the contrary, the results of synthetic tests always reject the null-hypothesis for $\alpha = 5\%$.

Finally, the possible impact of the earthquake clusters (as also discussed in Michael [1997]) on achieved results has been also evaluated by performing the Molchan analysis assuming random forecasts. To accomplish this purpose, we preserved the spatial features of the SSTAs and their time duration while randomly generating the starting time of each SSTA. In this way, we generated 50 collections of synthetic SSTAs. Figure 6(b) shows the results of the Molchan analysis; just the average of the results achieved on synthetic shuffled SSTAs is reported. Both the average (in Figure 6(b)) and all the results (see Table S4 in supporting information) of such an analysis fall in the not optimistic area of the error diagram; both of them reject the null-hypothesis at the significant level $\alpha = 5\%$. It should be noted that occasional values of G (up to 1.9) have also been recorded, even if they are always less than the corresponding ones achieved on real data.

4. Toward a Multiparametric Approach

The performed analyses indicate that achieved results do not depend on the spatial–temporal distribution of earthquakes. In addition, they indicate that a noncasual correlation (in comparison with the random guess function, see Zechar and Jordan, 2008, and references therein) exists between SSTAs and M6 earthquakes. These circumstances suggest that "RST-based satellite thermal anomalies" can be considered as one of the parameters to be included in a multiparametric system for the assessment of seismic hazard in the short term (t-DASH; Tramutoli et al., 2014).

A multiparametric approach, where it is possible to combine the "earthquake forecast" capabilities of non-seismological and seismological parameters, could be considered as a promising way for improving our capabilities to estimate future earthquake probabilities. Up to now, proposed OEF methods suffer from strong limitations in terms of their actual (too low absolute values of estimated probabilities) and general (forecast is substantially limited to earthquakes that are preceded by foreshocks) operational applicability (e.g., Panza et al., 2014; Wang & Rogers, 2014). Aiming at maximizing the overall predictive skill of such methods, several authors proposed some "multiparametric approaches" based on a combination of forecasting models. For example, Sobolev et al. (1991) use Bayes formula for conditional probabilities, Rhoades and Gerstenberger (2009) suggest to combine models by means of a weighted mean, while Rhoades et al. (2014) and Shebalin et al. (2014) propose, respectively, a multiplicative structure for combining models and/or earthquake precursors. Nakatami (2020) suggests a different approach, which takes account of the space–time volume occupied by the alarms rather than the number of alarms/anomalies.

We expect a strong reduction of the alerted space–time volumes (Figure 7), as well as a progressive reduction of the combined probabilities of false alarms, by combining multiparametric observations. In fact, being

- $P_{V_i}(M)$ the probability (previously estimated and based on a long-term correlation analysis concerning the ith parameter) that an earthquake of magnitude equal to or greater than M occurs within the area A_i and time interval T_i, that is, within the alerted volume $V_i = A_i \cdot T_i$.
- V the volume that is contemporaneously alerted by N parameters, that is, the intersection of the volumes that are individually alerted by each considered parameter, with

$$V = \bigcap_1^N \left(A_i . T_i\right) = \bigcap_1^N V_i \tag{6}$$

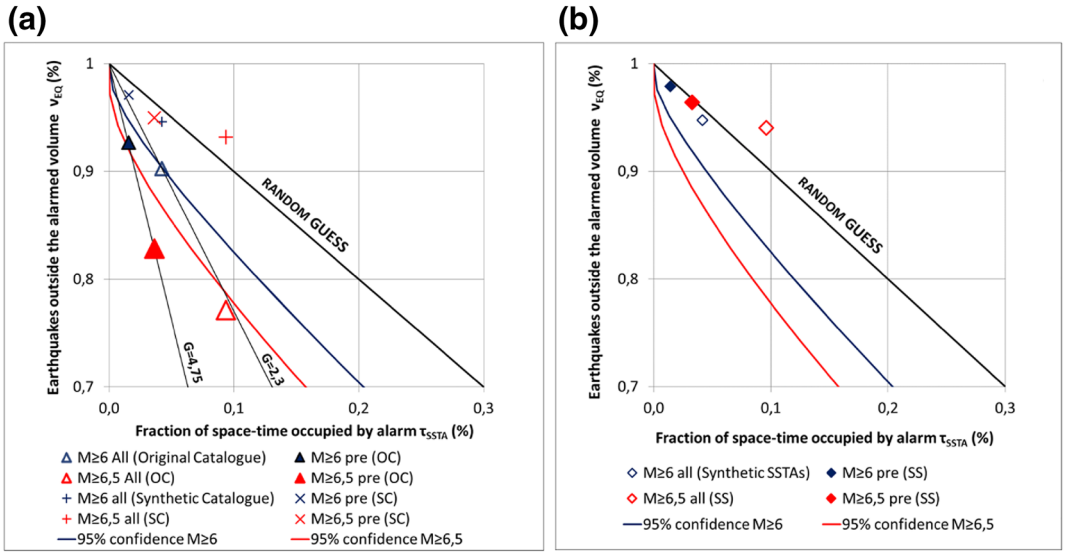

Figure 6. (a) Error diagram related to the analysis carried out with the earthquake catalog filtered on a monthly basis. As in Figure 5(a), results of the analyses performed by using synthetic catalogs (see Table S3 in supporting information) are also reported through their mean values. Symbol meaning is the same as in Figure 5(a). (b) Error diagram concerning the analysis carried out, taking random forecast (i.e., synthetic SSTAs) into account. The analysis has been performed considering as "target" the events belonging to the filtered monthly catalog. Blue and red rhombi indicate the mean values of results concerning the analyses performed by using synthetic SSTAs. Table S4 of the supporting information reports full details of the analysis. SSTAs, Significant Sequence of Thermal Anomalies.

the joint probability $P_J(M)$ that an earthquake of magnitude equal to or greater than M occurs in the volume V can be computed as in the following expression:

$$P_J(M) = 1 - \prod_{i=1}^{N}\left[1 - P_{V_i}(M)\cdot\frac{V}{V_i}\right] \tag{7}$$

where we assume that false positives are associated with independent processes.

Observations to be included in a multiparametric system will be selected taking account of indications

- from the physical models that were proposed to explain the relations among the different parameters (seismological and not) in the different stages of the earthquake process and
- provided by long-term correlation analyses from which $P_{V_i}(M)$ values, describing "earthquakes forecast" capabilities of each parameter, can be obtained.

As an example, the LAIC model (Pulinets & Ouzounov, 2011) and its subsequent reinterpretations (e.g., Kuo et al., 2014) describe the link between different atmospheric and ionospheric parameters and how they couple with each other during the final stage of the seismic process. For example, in the mechanism proposed by Pulinets and Ouzounov (2011), the fault activation can bring to an anomalous ionization (due to intensive radon gas emission) of the near-surface air, which could trigger different measurable anomalies in different layers of the atmosphere and ionosphere. For instance, the literature (e.g., Pulinets et al., 2018) reports the expected appearance in a specific time sequence of anomalous changes in emitted longwave infrared radiation, electric field, relative humidity, geochemical potential, etc., before earthquake occurrence.

However, long-term studies are required in order to evaluate the forecasting potential of each candidate parameter in terms of successful forecasts, false-positive rates, and/or missed events. Moreover, they should clearly indicate the magnitude constraints as well as the corresponding alerted space–time volume to be used—together with the relative weight (in terms of earthquake occurrence probability) computed for each investigated region—in a multiparametric earthquake forecasting system.

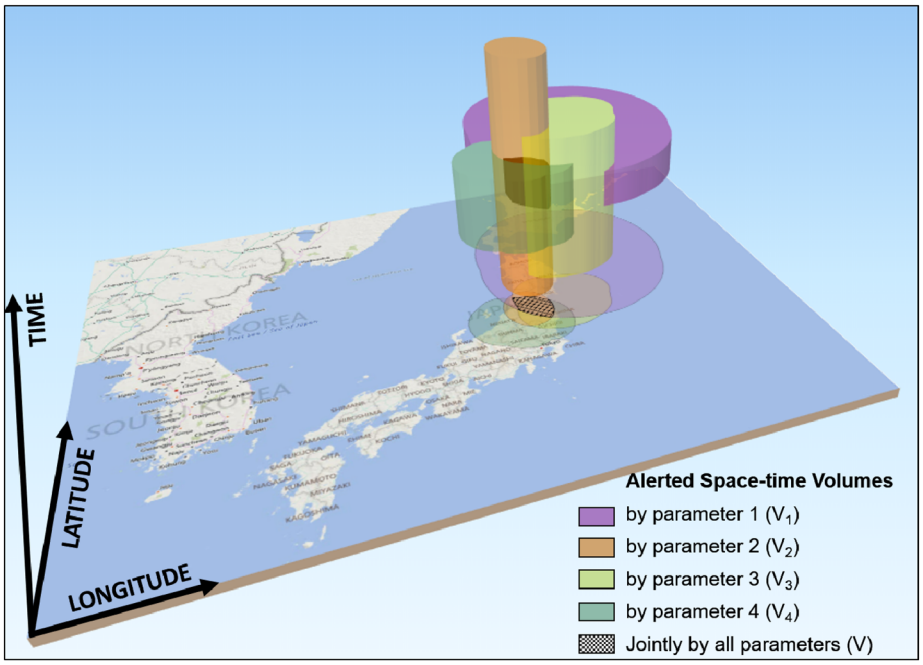

Figure 7. The schematic 3D representation of the reduction of the alerted space–time volume by a multiparametric approach. Colored cylinders represent the "alerted" space–time volumes V_i of each (nonseismological and seismological) parameter i. The intersection V of these cylinders identifies the jointly "alerted" space–time volume as a result of the integration of multiparametric observations.

For example, considering the Japanese country, in addition to this study on satellite thermal anomalies, long-term correlation analyses have been performed by:

- Wang et al. (2013) on daily GPS measurements of ground deformation in the Kanto area (Central Japan) from 1999 to 2009, they show a probability gain of 2–4 against a Poisson model, with a false alarm rate lower than 50%, for earthquakes with magnitude $M \geq 5.5$.
- Hattori et al. (2013) and Han et al. (2014, 2017) on 10 years (2001–2010) of geomagnetic data recorded in some stations around the Kanto region, they highlight that ULF seismomagnetic phenomena occur weeks to days before moderate–large earthquakes in an area of 100/150 km from the station. In particular, Han et al. (2014) record a probability gain of 1.6 against a random guess for data observed at the Kakioka station.
- Hayakawa et al. (2010) on 7 years (2001–2007) of VLF/LF data, they highlight that subionospheric perturbations take place from a few days to 1 week before the occurrence of M6 earthquakes with shallow depth (<40 km).
- Kon et al. (2011) on GIM-TEC maps, they show on selected $M \geq 6$ earthquakes that TEC anomalies appear from 5 days to 1 day before earthquake occurrence within 1,000 km from the epicenter in the period May 1998–2010.

Although some of these parameters need to be better qualified, for example, in terms of false-positive rates and achievable probability gain, the aforementioned studies could represent a preliminary step toward a multiparametric t-DASH system for Japan or at least part of it (e.g., Kanto area).

5. Conclusions

The integration of different observations in a multiparametric approach could improve our present knowledge on the earthquake-related processes and accelerate the development of an operational t-DASH system. The set-up of a multiparametric system preliminary requires

1. recognizing those parameters that exhibit significant (in a statistical sense) variations in a possible relation (based on suitable physical models and/or experimental observations) with the preparation process of earthquakes;
2. measuring the candidate parameters with a sufficient space–time continuity;
3. identifying the well-founded and repeatable data processing techniques that are able to discriminate seismic signatures from other variations;
4. establishing the correlation level (based on long-term analyses) between such observational signatures and earthquake occurrences (time, position, magnitude, etc.); and
5. evaluating the impact (i.e., the actual information content even in comparison with random guesses) of the considered parameter in a t-DASH multiparameter system.

In this paper, we followed those five steps in order to verify whether or not the "RST-based TIR anomalies" could be a suitable candidate for a t-DASH system. To this aim, we used nighttime thermal images, obtained by the JAMI and IMAGER satellite sensors, on board the MTSAT-1R and -2 geostationary platforms, over the Japanese territory, during July 2005 to December 2015 period, to perform a long-term analysis (11 years) based on the RST approach. Moreover, to reduce the proliferation of the TIR anomalies produced by causes (i.e., false-positive TAs) independent from the seismic activity (e.g., variable cloud coverage), we introduced a new scheme (i.e., MWC instead of the traditional FWC) for computing the RST reference fields.

The long-term RST analysis indicates that

- SSTAs have a very sporadic occurrence; only 1.8% of all TIR satellite images show the presence of SSTAs.
- Applying the newly proposed scheme to compute the RST reference fields, a reduction of false-positive TAs has been achieved (from 50% to 37.9%). In particular, false positives fall down to zero in selected areas.
- Based on a clear definition of SSTA and well-defined validation rules, the performed correlation analysis revealed that 62.1% of them are within the preestablished space–time span from the earthquake (with $M_{JMA} \geq 6$) epicenter and occurrence time. A marked tendency is found for SSTAs to appear before earthquake occurrences (70% of the ones related to earthquakes).
- The results of the error diagram show a noncasual correlation. In particular, for large earthquakes, we record a probability gain up to 4.3 against the random guess when the temporal window of 1 day is used for the declustering.
- The extension of 1 month of declustering temporal window, as expected, does not significantly change the results. False positives increase from 37.9% up to 41.3% and probability gain from 4.3 up to 4.75.

Acknowledgments
The paper is part of achievements during N.G.'s visit under JSPS postdoctoral fellowships for research in Japan, and it is cofunded by the Center for Environmental Remote Sensing of Chiba University (Japan) by means of a joint research program and the Ministry of Education, Culture, Sports, Science and Technology (MEXT) of Japan,under its Observation and Research Program for Prediction of Earthquakes and Volcanic Eruptions. N.G. especially thanks JSPS and the Graduate School of Science of Chiba University for providing such an opportunity. The research leading to these results is also part of the continuation of the EC-FP7 PRE-EARTHQUAKES (Processing Russian and European EARTH observations for earthQUAKE precursors Studies) project activities, G.A.n. 263502. The authors acknowledge valuable support from the Center for Environmental Remote Sensing to provide thermal infrared data on MTSATs and thank the Japan Meteorological Agency for seismic data.

Data Availability Statement

Thermal infrared data on MTSATs available online at ftp://mtsat.cr.chiba-u.ac.jp/ and seismic data available online at http://www.jma.go.jp/en/quake/quake_singen_index.html.

References

Akhoondzadeh, M. (2013). A comparison of classical and intelligent methods to detect potential thermal anomalies before the 11 August 2012 Varzeghan, Iran, earthquake (Mw = 6.4). *Natural Hazards and Earth System Science*, *13*(4), 1077–1083. https://doi.org/10.5194/nhess-13-1077-2013

Aki, K. (1989). Ideal probabilistic earthquake prediction. *Tectonophysics*, *169*(1–3), 197–198. https://doi.org/10.1016/0040-1951(89)90193-5

Aliano, C., Corrado, R., Filizzola, C., Genzano, N., Pergola, N., & Tramutoli, V. (2008a). Robust TIR satellite techniques for monitoring earthquake active regions: Limits, main achievements and perspectives. *Annales Geophysicae*, *51*(1), 303–317. https://doi.org/10.4401/ag-3050

Aliano, C., Corrado, R., Filizzola, C., Pergola, N., & Tramutoli, V. (2008b). Robust satellite techniques (RST) for the thermal monitoring of earthquake prone areas: The case of Umbria-Marche October, 1997 seismic events. *Annales Geophysicae*, *51*(2/3), 451–459.

Barka, A. (1999). The 17th August 1999 Izmit Earthquake. *Science*, *285*, 1858–1859.

Bellaoui, M., Hassini, A., & Bouchouicha, K. (2017). Pre-seismic anomalies in remotely sensed land surface temperature measurements: The case study of 2003 Boumerdes earthquake. *Advances in Space Research*, *59*(10), 2645–2657. https://doi.org/10.1016/j.asr.2017.03.004

Bonfanti, P., Genzano, N., Heinicke, J., Italiano, F., Martinelli, G., Pergola, N., et al. (2012). Evidence of CO_2-gas emission variations in the central Apennines (Italy) during the L'Aquila seismic sequence (March–April 2009). *Bollettino di Geofisica Teorica ed Applicata*, *53*(1), 147–168.

Chiodini, G., Caliro, S., Cardellini, C., Frondini, F., Inguaggiato, S., & Matteucci, F. (2011). Geochemical evidence for and characterization of CO2 rich gas sources in the epicentral area of the Abruzzo 2009 earthquakes. *Earth and Planetary Science Letters*, *304*(3-4), 389–398. https://doi.org/10.1016/j.epsl.2011.02.016

Cicerone, R. D., Ebel, J. E., & Britton, J. (2009). A systematic compilation of earthquake precursors. *Tectonophysics*, *476*, 371–396. https://doi.org/10.1016/j.tecto.2009.06.008

Cuomo, V., Filizzola, C., Pergola, N., Pietrapertosa, C., & Tramutoli, V. (2004). A self-sufficient approach for GERB cloudy radiance detection. *Atmospheric Research*, *72*, 39–56.

Dobrovolsky, I. P., Zubkov, S. I., & Miachkin, V. I. (1979). Estimation of the size of earthquake preparation zones. *Pure and Applied Geophysics PAGEOPH*, *117*, 1025–1044. https://doi.org/10.1007/BF00876083

Doglioni, C., Barba, S., Carminati, E., & Riguzzi, F. (2014). Fault on–off versus coseismic fluids reaction. *Geoscience Frontiers*, *5*, 767–780.

Eleftheriou, A., Filizzola, C., Genzano, N., Lacava, T., Lisi, M., Paciello, R., et al. (2016). Long-term RST analysis of anomalous TIR sequences in relation with earthquakes occurred in Greece in the period 2004–2013. *Pure and Applied Geophysics*, *173*(1), 285–303. https://doi.org/10.1007/s00024-015-1116-8

Eneva, M. D., Adams, N., Wechsler, Y., Ben-Zion, Y., & Dor, O. (2008). Thermal properties of faults in Southern California from remote sensing data (Report sponsored by NASA under contract to SAIC No. NNH05CC13C, p. 70). Greenbelt, MD: NASA Goddard Space Flight Center.

Filizzola, C., Pergola, N., Pietrapertosa, C., & Tramutoli, V. (2004). Robust satellite techniques for seismically active areas monitoring: A sensitivity analysis on September 7, 1999 Athens's earthquake. *Physics and Chemistry of the Earth*, *29*(4–9), 517–527. https://doi.org/10.1016/j.pce.2003.11.019

Freund, F. T. (2007). Pre-earthquake signals—Part I: Deviatoric stresses turn rocks into a source of electric currents. *Natural Hazards and Earth System Sciences*, *7*, 535–541.

Fu, C. C., Lee, L. C., Ouzounov, D., & Jan, J. C. (2020). Earth's outgoing longwave radiation variability prior to M ≥ 6.0 earthquakes in the Taiwan area during 2009–2019. *Frontiers in Earth Science*, *8*, 364. 1–15. https://doi.org/10.3389/feart.2020.00364

Geller, R. J. (1997). Earthquake prediction: A critical review. *Geophysical Journal International*, *131*, 425–450.

Genzano, N., Aliano, C., Corrado, R., Filizzola, C., Lisi, M., Mazzeo, G., et al. (2009). RST analysis of MSG-SEVIRI TIR radiances at the time of the Abruzzo 6 April 2009 earthquake. *Natural Hazards and Earth System Sciences*, *9*, 2073–2084. https://doi.org/10.5194/nhess-9-2073-2009

Genzano, N., Filizzola, C., Lisi, M., Pergola, N., & Tramutoli, V. (2020). Toward the development of a multi parametric system for a short-term assessment of the seismic hazard in Italy. *Annales Geophysicae*, *63*(5), PA550. https://doi.org/10.4401/ag-8227

Genzano, N., Filizzola, C., Paciello, R., Pergola, N., & Tramutoli, V. (2015). Robust Satellite Techniques (RST) for monitoring earthquake prone areas by satellite TIR observations: The case of 1999 Chi-Chi earthquake (Taiwan). *Journal of Asian Earth Sciences*, *114*, 289–298. https://doi.org/10.1016/j.jseaes.2015.02.010

Halle, W., Oertel, D., Schlotzhauer, G., & Zhukov, B. (2008). *Early warning of earthquakes by space-borne infrared sensors* [Erdbebenfrüherkennung mit InfraRot Sensoren aus dem Weltraum] (pp. 1–106). Berlin-Adlershof: DLR. https://elib.dlr.de/58678/

Han, P., Hattori, K., Hirokawa, M., Zhuang, J., Chen, C. H., Febriani, F., et al. (2014). Statistical analysis of ULF seismo-magnetic phenomena at Kakioka, Japan, during 2001–2010. *Journal of Geophysical Research: Space Physics*, *119*, 4998–5011. https://doi.org/10.1002/2014JA019789

Han, P., Hattori, K., Zhuang, J., Chen, C. H., Liu, J.-Y., & Yoshida, S. (2017). Evaluation of ULF seismo-magnetic phenomena in Kakioka, Japan by using Molchan's error diagram. *Geophysical Journal International*, *208*, 482–490. https://doi.org/10.1093/gji/ggw404

Han, P., Zhuang, J., Hattori, K., Chen, C. H., Febriani, F., Chen, H., et al. (2020). Assessing the potential earthquake precursory information in ULF magnetic data recorded in Kanto, Japan during 2000–2010: Distance and magnitude dependences. *Entropy*, *22*, 859. https://doi.org/10.3390/e22080859

Hattori, K., Han, P., Yoshino, C., Febriani, F., Yamaguchi, H., & Chen, C. H. (2013). Investigation of ULF seismo-magnetic phenomena in Kanto, Japan During 2000–2010: Case studies and statistical studies. *Surveys in Geophysics*, *34*, 293–316. https://doi.org/10.1007/s10712-012-9215-x

Hayakawa, M., Kasahara, Y., Nakamura, T., Muto, F., Horie, T., Maekawa, S., et al. (2010). A statistical study on the correlation between lower ionospheric perturbations as seen by subionospheric VLF/LF propagation and earthquakes. *Journal of Geophysical Research*, *115*, A09305. https://doi.org/10.1029/2009JA015143

Heinicke, J., Martinelli, G., & Telesca, L. (2011). Geodynamically induced variations in the emission of CO_2 gas at San Faustino (Central Apennines, Italy). *Geofluids*, *12*, 123–132.

Irwin, W. P., & Barnes, I. (1980). Tectonic relations of carbon dioxide discharges and earthquakes. *Journal of Geophysical Research*, *85*, 3115–3121.

Japan Meteorological Agency. (2021). *JMA (Japan Meteorological Agency) seismic catalogue*. http://www.data.jma.go.jp/svd/eqev/data/bulletin/index_e.html

Jiao, J. X., Zhao, Z. H., & Shan (2018). Pre-seismic anomalies from optical satellite observations: A review. *Natural Hazards and Earth System Sciences*, *18*, 1013–1036. https://doi.org/10.5194/nhess-18-1013-2018

Ke, F., Wang, Y., Wang, X., Qian, H., & Shi, C. (2016). Statistical analysis of seismo-ionospheric anomalies related to Ms > 5.0 earthquakes in China by GPS TEC. *Journal of Seismology*, *20*(1), 137–149.

Khalili, M., Panah, S. K. A., & Eskandar, S. S. A. (2019). Using Robust Satellite Technique (RST) to determine thermal anomalies before a strong earthquake: A case study of the Saravan earthquake (April 16th, 2013, MW = 7.8, Iran). *Journal of Asian Earth Sciences*, *173*, 70–78. https://doi.org/10.1016/j.jseaes.2019.01.009

Kon, S., Nishihashi, M., & Hattori, K. (2011). Ionospheric anomalies possibly associated with M ≥ 6.0 earthquakes in the Japan area during 1998–2010: Case studies and statistical study. *Journal of Asian Earth Sciences*, *41*, 410–420. https://doi.org/10.1016/j.jseaes.2010.10.005

Kossobokov, V., & Shebalin, P. (2003). Earthquake prediction. In V. I. Keilis-Borok & A. A. Soloviev (Eds.), *Nonlinear dynamics of the lithosphere and earthquake prediction* (pp. 141–205). Berlin/Heidelberg, Germany: Springer.

Kossobokov, V. G. (2006). Testing earthquake prediction methods: "The West Pacific short-term forecast of earthquakes with magnitude MwHRV ≥5.8". *Tectonophysics*, 413, 25–31.

Kuo, C. L., Lee, L. C., & Huba, J. D. (2014). An improved coupling model for the lithosphere–atmosphere–ionosphere system. *Journal of Geophysical Research: Space Physics*, *119*, 3189–3205. https://doi.org/10.1002/2013JA019392

Le, H., Liu, J. Y., & Liu, L. (2011). A statistical analysis of ionospheric anomalies before 736 M6.0+ earthquakes during 2002–2010. *Journal of Geophysical Research*, *116*, A02303. https://doi.org/10.1029/2010JA015781

Li, J., Wu, L., Dong, Y., Liu, S., & Yang, X. (2007). An quantitative model for tectonic activity analysis and earthquake magnitude predication based on thermal infrared anomaly. In *International geoscience and remote sensing symposium (IGARSS)* (pp. 3039–3042). https://doi.org/10.1109/IGARSS.2007.4423485

Li, M., & Parrot, M. (2013). Statistical analysis of an ionospheric parameter as a base for earthquake prediction. *Journal of Geophysical Research: Space Physics*, *118*, 3731–3739. https://doi.org/10.1002/jgra.50313

Lisi, M., Filizzola, C., Genzano, N., Grimaldi, C. S. L., Lacava, T., Marchese, F., et al. (2010). A study on the Abruzzo 6 April 2009 earthquake by applying the RST approach to 15 years of AVHRR TIR observations. *Natural Hazards and Earth System Sciences*, *10*, 395–406. https://doi.org/10.5194/nhess-10-395-2010

Liu, J. Y., Chen, C. H., Chen, V. I., Yang, W. H., Oyama, K. I., & Kuo, K. W. (2010). A statistical study of ionospheric earthquake precursors monitored by using equatorial ionization anomaly of GPS TEC in Taiwan during 2001–2007. *Journal of Asian Earth Sciences*, *39*(1), 76–80.

Liu, J. Y., Chen, Y. I., Chuo, Y. J., & Chen, C. S. (2006). A statistical investigation of preearthquake ionospheric anomaly. *Journal of Geophysical Research*, *111*, A05304. https://doi.org/10.1029/2005JA011333

Liu, J. Y., Chen, Y. I., Huang, C. H., Ho, Y. Y., & Chen, C. H. (2015). A statistical study of lightning activities and M ≥ 5.0 earthquakes in Taiwan during 1993–2004. *Surveys in Geophysics*, *36*(6), 851–859.

Lucente, F. P., Gori, P. D., Margheriti, L., Piccinini, D., Bona, M. D., Chiarabba, C., & Agostinetti, N. P. (2010). Temporal variation of seismic velocity and anisotropy before the 2009 MW 6.3 L'Aquila earthquake, Italy. *Geology*, *38*, 1015–1018.

Martinelli, G., Facca, G., Genzano, N., Gherardi, F., Lisi, M., Pierotti, L., & Tramutoli, V. (2020). Earthquake-related signals in central Italy detected by hydrogeochemical and satellite techniques. *Frontiers of Earth Science*, *8*, 584716. https://doi.org/10.3389/feart.2020.584716

Michael, A. J. (1997). Testing prediction methods: Earthquake clustering versus the Poisson model. *Geophysical Research Letters*, *24*, 1891–1894.

Molchan, G. (2012). On the testing of seismicity models. *Acta Geophysica*, *60*(3), 624–637. https://doi.org/10.2478/s11600-011-0042-0

Molchan, G. M. (1990). Strategies in strong earthquake prediction. *Physics of the Earth and Planetary Interiors*, *61*, 84–98.

Molchan, G. M. (1991). Structure of optimal strategies in earthquake prediction. *Tectonophysics*, *193*(4), 267–276. https://doi.org/10.1016/0040-1951(91)90336-Q

Molchan, G. M. (1997). Earthquake prediction as a decision-making problem. *Pure and Applied Geophysics PAGEOPH*, *149*(1), 233–247. https://doi.org/10.1007/BF00945169

Molchan, G. M., & Kagan, Y. Y. (1992). Earthquake prediction and its optimization. *Journal of Geophysical Research*, *97*, 4823. https://doi.org/10.1029/91JB03095

Mukhopadhyay, U. K., Sharma, R. N. K., Anwar, S., & Dutta, A. D. (2021). Earthquakes and thermal anomalies in a remote sensing perspective. In A. E. Hassanien & A. Darwish (Eds.), *Machine learning and big data analytics paradigms: Analysis, applications and challenges. Studies in big data* (Vol. *77*). Cham, Switzerland: Springer. https://doi.org/10.1007/978-3-030-59338-4_11

Nakatami, M. (2020). Evaluation of phenomena preceding earthquakes and earthquake predictability. *Journal of Disaster Research*, *15*(2), 112–143.

Panza, G., Kossobokov, V. G., Peresan, A., & Nekrasova, A. (2014). Why are the standard probabilistic methods of estimating seismic hazard and risks too often wrong, earthquake hazard, risk and disasters. *Earthquake Hazard, Risk and Disasters* (pp. 309–357). Amsterdam, Netherlands: Elsevier. https://doi.org/10.1016/B978-0-12-394848-9.00012-2

Pergola, N., Aliano, C., Coviello, I., Filizzola, C., Genzano, N., Lacava, T., et al. (2010). Using RST approach and EOS-MODIS radiances for monitoring seismically active regions: A study on the 6 April 2009 Abruzzo earthquake. *Natural Hazards and Earth System Sciences*, *10*, 239–249. https://doi.org/10.5194/nhess-10-239-2010

Piscini, A., De Santis, A., Marchetti, D., & Cianchini, G. (2017). A multi-parametric climatological approach to study the 2016 Amatrice–Norcia (Central Italy) earthquake preparatory phase. *Pure and Applied Geophysics*, *174*(10), 3673–3688. https://doi.org/10.1007/s00024-017-1597-8

Pulinets, S. A., & Ouzounov, D. (2011). Lithosphere–Atmosphere–Ionosphere Coupling (LAIC) model—An unified concept for earthquake precursors validation. *Journal of Asian Earth Sciences*, *41*, 371–382.

Pulinets, S. A., Ouzounov, D., Karelin, A. V., & Davidenko, D. V. (2018). Lithosphere–atmosphere–ionosphere–magnetosphere coupling—A concept for pre-earthquake signals generation. In D. Ouzounov, S. Pulinets, K. Hattori, & P. Taylor (Eds.), *Pre-earthquake processes: A multidisciplinary approach to earthquake prediction studies. Geophysical monograph series* (pp. 79–98). AGU Publication; Hoboken, NJ: John Wiley & Sons, Inc.; Washington, D. C: Geophysical Union.

Qiang, Z., Xu, X., & Dian, C. (1997). Case 27 thermal infrared anomaly precursor of impending earthquakes. *Pure and Applied Geophysics*, *149*, 159–171. https://doi.org/10.1007/BF00945166

Rhoades, D. A., & Gerstenberger, M. C. (2009). Mixture models for improved short-term earthquake forecasting. *Bulletin of the Seismological Society of America*, *99*, 636–646. https://doi.org/10.1785/0120080063

Rhoades, D. A., Gerstenberger, M. C., Christophersen, A., Zechar, J. D., Schorlemmer, D., Werner, M. J., & Jordan, T. H. (2014). Regional earthquake likelihood models II: Information gains of multiplicative hybrids. *Bulletin of the Seismological Society of America*, *104*(6), 3072–3083. https://doi.org/10.1785/0120140035

Scholz, C. H., Sykes, L. R., & Aggarwal, Y. P. (1973). Earthquake prediction: A physical basis. *Science*, *181*, 803–810.

Schorlemmer, D., Werner, M. J., Marzocchi, W., Jordan, T. H., Ogata, Y., Jackson, D. D., et al. (2018). The collaboratory for the study of earthquake predictability: Achievements and priorities. *Seismological Research Letters*, *89*(4), 1305–1313. https://doi.org/10.1785/0220180053

Shah, M., & Jin, S. (2015). Statistical characteristics of seismoionospheric GPS TEC disturbances prior to global Mw ≥ 5.0 earthquakes (1998–2014). *Journal of Geodynamics*, *92*, 42–49.

Shebalin, P., Keilis-Borok, V., Gabrielov, A., Zaliapin, I., & Turcotte, D. (2006). Short-term earthquake prediction by reverse analysis of lithosphere dynamics. *Tectonophysics*, *413*, 63–75. https://doi.org/10.1016/j.tecto.2005.10.033

Shebalin, P. N. (2018). Combining probabilistic seismicity models with precursory information. In D. Ouzounov, S. Pulinets, K. Hattori, & P. Taylor (Eds.), *Pre-earthquake processes: A multidisciplinary approach to earthquake prediction studies. Geophysical monograph series* (pp. 173–195). AGU Publication; Hoboken, NJ: John Wiley & Sons, Inc.; Washington, D. C: Geophysical Union.

Shebalin, P. N., Narteau, C., Zechar, J., & Holschneider, M. (2014). Combining earthquake forecasts using differential probability gains. *Earth, Planets and Space*, *66*, 37. https://doi.org/10.1186/1880-5981-66-37

Sobolev, G. A., Chelidze, T. L., Zavyalov, A. D., Slavina, L. B., & Nikoladze, V. E. (1991). Maps of expected earthquakes based on a combination of parameters. *Tectonophysics*, *193*, 255–265. https://doi.org/10.1016/0040-1951(91)90335-P

Tamburello, G., Pondrelli, S., Chiodini, G., & Rouwet, D. (2018). Global-scale control of extensional tectonics on CO_2 Earth degassing. *Nature Communications*, *9*, 4608.

Thomas, J. N., Huard, J., & Masci, F. (2017). A statistical study of global ionospheric map total electron content changes prior to occurrences of M ≥ 6.0 earthquakes during 2000–2014. *Journal of Geophysical Research: Space Physics*, *122*, 2151–2161. https://doi.org/10.1002/2016JA023652

Tramutoli, V. (1998). Robust AVHRR Techniques (RAT) for environmental monitoring: Theory and applications. In G. Cecchi & E. Zilioli (Eds.), *Proceedings of SPIE* (Vol. 3496, pp. 101–113). Earth surface remote sensing II. Published in SPIE Proceedings. https://doi.org/10.1117/12.332714

Tramutoli, V. (2007). Robust satellite techniques (RST) for natural and environmental hazards monitoring and mitigation: Theory and applications. In *2007 international workshop on the analysis of multi-temporal remote sensing images* (pp. 1–6). IEEE. https://doi.org/10.1109/MULTITEMP.2007.4293057

Tramutoli, V., Aliano, C., Corrado, R., Filizzola, C., Genzano, N., Lisi, M., et al. (2009). Abrupt change in greenhouse gases emission rate as a possible genetic model of TIR anomalies observed from satellite in earthquake active regions. In *Proceedings, 33rd International Symposium on Remote Sensing of Environment (ISRSE33)* (pp. 567–570). ISRSE 2009: Stresa; Italy; 4 May 2009 to 8 May 2009

Tramutoli, V., Aliano, C., Corrado, R., Filizzola, C., Genzano, N., Lisi, M., et al. (2013). On the possible origin of thermal infrared radiation (TIR) anomalies in earthquake-prone areas observed using robust satellite techniques (RST). *Chemical Geology*, *339*, 157–168. https://doi.org/10.1016/j.chemgeo.2012.10.042

Tramutoli, V., Corrado, R., Filizzola, C., Genzano, N., Lisi, M., Paciello, R., & Pergola, N. (2015). One year of RST based satellite thermal monitoring over two Italian seismic areas. *Bollettino di Geofisica Teorica ed Applicata*, *56*(June), 275–294. https://doi.org/10.4430/bgta0150

Tramutoli, V., Corrado, R., Filizzola, C., Genzano, N., Lisi, M., & Pergola, N. (2015). From visual comparison to robust satellite techniques : 30 years of thermal infrared satellite data analyses for the study of earthquake preparation phases. *Bollettino di Geofisica Teorica ed Applicata*, *56*(June), 167–202. https://doi.org/10.4430/bgta0149

Tramutoli, V., Cuomo, V., Filizzola, C., Pergola, N., & Pietrapertosa, C. (2005). Assessing the potential of thermal infrared satellite surveys for monitoring seismically active areas: The case of Kocaeli (İzmit) earthquake, August 17, 1999. *Remote Sensing of Environment*, *96*(3–4), 409–426. https://doi.org/10.1016/j.rse.2005.04.006

Tramutoli, V., Filizzola, C., Genzano, N., & Lisi, M. (2018). Robust satellite techniques for detecting pre-seismic thermal anomalies. In D. Ouzounov, S. Pulinets, K. Hattori, & P. Taylor (Eds.), *Pre-earthquake processes: A multidisciplinary approach to earthquake prediction studies. Geophysical monograph series* (pp. 234–258). AGU Publication; Hoboken, NJ: John Wiley & Sons, Inc.; Washington, D. C: Geophysical Union.

Tramutoli, V., Jakowski, N., Pulinets, S., Romanov, A., Filizzola, C., Shagimuratov, I., et al. (2014). From PRE-EARTQUAKES to EQUOS: How to exploit multi-parametric observations within a novel system for time-dependent assessment of seismic hazard (T-DASH) in a pre-operational civil protection context. Paper presented at Proceedings of Second European Conference on Earthquake Engineering and Seismology (2ECEES), Turkey, August 24–29, 2014.

Tramutoli, V., & Vallianatos, F. (2020). Foreword: Advances in multi-parametric, time-dependent assessment of seismic hazard and earthquakes forecast. *Annals of Geophysics*, *63*(5), 1–5. https://doi.org/10.4401/ag-8594

Tronin, A. A. (1996). Satellite thermal survey—A new tool for the study of seismoactive regions. *International Journal of Remote Sensing*, *17*, 1439–1455.

Tronin, A. A. (2006). Remote sensing and earthquakes: A review. *Physics and Chemistry of the Earth*, *31*, 138–142. https://doi.org/10.1016/j.pce.2006.02.024

Wang, K., & Rogers, G. C. (2014). Earthquake preparedness should not fluctuate on a daily or weekly basis. *Seismological Research Letters*, *85*(3), 569–571. https://doi.org/10.1785/0220130195

Wang, T., Zhuang, J., Kato, T., & Bebbington, M. (2013). Assessing the potential improvement in short-term earthquake forecasts from incorporation of GPS data. *Geophysical Research Letters*, *40*, 2631–2635. https://doi.org/10.1002/grl.50554

Xiong, P., Gu, X. F., Bi, Y. X., Shen, X. H., Meng, Q. Y., Zhao, L. M., et al. (2013). Detecting seismic IR anomalies in bi-angular advanced along-track scanning radiometer data. *Natural Hazards and Earth System Sciences*, *13*(8), 2065–2074. https://doi.org/10.5194/nhess-13-2065-2013

Zechar, J. D., & Jordan, T. H. (2008). Testing alarm-based earthquake predictions. *Geophysical Journal International*, *172*(2), 715–724. https://doi.org/10.1111/j.1365-246X.2007.03676.x

Zechar, J. D., & Jordan, T. H. (2010). The area skill score statistic for evaluating earthquake predictability experiments. *Pure and Applied Geophysics*, *167*(2010), 893–906. https://doi.org/10.1007/s00024-010-0086-0

Zhang, Y., & Meng, Q. (2019). A statistical analysis of TIR anomalies extracted by RSTs in relation to an earthquake in the Sichuan area using MODIS LST data. *Natural Hazards and Earth System Sciences*, *19*, 535–549. https://doi.org/10.5194/nhess-19-535-2019

Zhu, F., Su, F., & Lin, J. (2018). Statistical analysis of TEC anomalies prior to M6.0+ earthquakes during 2003–2014. *Pure and Applied Geophysics*, *175*(2018), 3441–3450. https://doi.org/10.1007/s00024-018-1869-y

Zhu, F., Zhou, Y., Lin, J., & Su, F. (2014). A statistical study on the temporal distribution of ionospheric TEC anomalies prior to M7.0+ earthquakes during 2003–2012. *Astrophysics and Space Science*, *350*(2), 449–457.